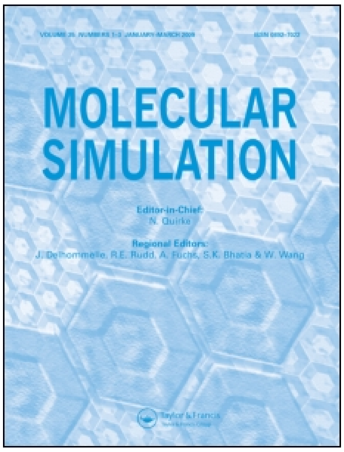


## Molecular Simulation
Publication details, including instructions for authors and subscription information:
http://www.informaworld.com/smpp/title~content=t713644482

# Thermal Properties of Supercritical Carbon Dioxide by Monte Carlo Simulations

C. M. Colina[ab]; C. G. Olivera-Fuentes[a]; F. R. Siperstein[b]; M. Lísal[cd]; K. E. Gubbins[b]
[a] TADiP Group, Thermodynamics and Transport Phenomena Department, Simón Bolívar University, Caracas, Venezuela [b] Chemical Engineering Department, North Carolina State University, Raleigh, NC, USA [c] E. Hála Laboratory of Thermodynamics Institute of Chemical Process Fundamentals, Academy of Sciences of the Czech Republic, Prague, Czech Republic [d] Department of Physics, J. E. Purkyne University, Czech Republic

Online publication date: 26 October 2010

**To cite this Article** Colina, C. M. , Olivera-Fuentes, C. G. , Siperstein, F. R. , Lísal, M. and Gubbins, K. E.(2003) 'Thermal Properties of Supercritical Carbon Dioxide by Monte Carlo Simulations', Molecular Simulation, 29: 6, 405 — 412

**To link to this Article: DOI:** 10.1080/0892702031000117135

**URL:** http://dx.doi.org/10.1080/0892702031000117135

*Molecular Simulation*, Vol. 29 (6–7), June 2003, pp. 405–412

Taylor & Francis
Taylor & Francis Group

# Thermal Properties of Supercritical Carbon Dioxide by Monte Carlo Simulations

C.M. COLINA[a,b,*], C.G. OLIVERA-FUENTES[a], F.R. SIPERSTEIN[b], M. LÍSAL[c,d] and K.E. GUBBINS[b]

[a]*TADiP Group, Thermodynamics and Transport Phenomena Department, Simón Bolívar University, Apartado Postal 89000, Caracas 1080, Venezuela;* [b]*Chemical Engineering Department, North Carolina State University, Raleigh, NC 27695, USA;* [c]*E. Hála Laboratory of Thermodynamics, Institute of Chemical Process Fundamentals, Academy of Sciences of the Czech Republic, Prague, Czech Republic;* [d]*Department of Physics, J. E. Purkyne University, 400 96 Usti n. Lab., Czech Republic*

*(Received September 2002; In final form January 2003)*



**We present simulation results for the volume expansivity, isothermal compressibility, isobaric heat capacity, Joule–Thomson coefficient and speed of sound for carbon dioxide ($CO_2$) in the supercritical region, using the fluctuation method based on Monte Carlo simulations in the isothermal–isobaric ensemble. We model $CO_2$ as a quadrupolar two-center Lennard–Jones fluid with potential parameters reported in the literature, derived from vapor–liquid equilibria (VLE) of $CO_2$. We compare simulation results with an equation of state (EOS) for the two-center Lennard–Jones plus point quadrupole (2CLJQ) fluid and with a multiparametric EOS adjusted to represent $CO_2$ experimental data. It is concluded that the VLE-based parameters used to model $CO_2$ as a quadrupolar two-center Lennard–Jones fluid (both simulations and EOS) can be used with confidence for the prediction of thermodynamic properties, including those of industrial interest such as the speed of sound or Joule–Thomson coefficient, for $CO_2$ in the supercritical region, except in the extended critical region.**

*Keywords*: Fluctuations; Carbon dioxide; 2CLJQ; Joule–Thomson coefficient; Speed of sound

## INTRODUCTION

Simulation methods that make use of force fields, parameterized on the basis of quantum mechanical calculations and/or experimental measurements, offer an immediate and practical alternative for the prediction of the properties of molecular fluids. The quality of a given force field model depends on its simplicity and transferability beyond the set of conditions that were used for the parameterization. Transferability may imply that the force field parameters for a given interaction site can be used in different molecules (e.g. the parameters used to describe a methyl group should be applicable in many organic molecules), or that the force field is transferable to different state points (e.g. pressure, temperature or composition) and to different properties (e.g. thermodynamic, structural or transport).

In general, for pure components, the transferability of a force field to different state points is tested against vapor–liquid equilibria (VLE), heats of vaporization, second virial coefficients and the prediction of mixture properties. Some work has focused on the evaluation of heat capacities from fluctuations in molecular simulations [1], since heat capacities are derivatives of the basic thermodynamic functions, and are usually not taken into account when obtaining model parameters from experimental data. In this work, we are interested in applying the two-center Lennard–Jones plus point quadrupole (2CLJQ) model for carbon dioxide ($CO_2$), with VLE-based parameters proposed by Möller and Fischer [2], to the computation of volumetric and thermal properties of $CO_2$ at supercritical conditions. The molecular simulation results are compared to an analytical equation of state (EOS), hereafter called the 2CLJQ EOS [3–5], and with the Span–Wagner [6] EOS. The 2CLJQ EOS is based on the Boublik–Nezbeda EOS and simulation results for two-center Lennard–Jones and 2CLJQ fluids. The Span–Wagner EOS is the current standard for $CO_2$ and it is accepted as essentially equivalent to experimental data.

*Corresponding author. Address: Chemical Engineering Department, North Carolina State University, Raleigh, NC 27695, USA. E-mail: ccolina@eos.ncsu.edu

ISSN 0892-7022 print/ISSN 1029-0435 online © 2003 Taylor & Francis Ltd
DOI: 10.1080/0892702031000117135

There have been a number of potential models proposed for $CO_2$, obtained from correlation of VLE properties [2,7–9], liquid properties [10], crystal structures and lattice properties [11], or from combinations of experimental data for non-bonded interactions and *ab initio* electrostatic potentials for charge distributions [12]. Several of these models have been used to study mixture properties [13–16], structural properties [17] and the pure component vapor–solid coexistence curve [18].

The 2CLJQ model for $CO_2$ offers an excellent balance between simplicity and accuracy for the description of pressure–volume–temperature (PVT) properties. The interaction parameters presented by Möller and Fischer [2] were optimized to describe VLE and the authors showed that good predictions for densities and enthalpies could be obtained using this potential in a temperature range between 230 and 570 K, and for pressures up to 400 MPa. Although the authors calculated thermodynamic derivatives such as the isothermal compressibility during the optimization process of the potential model, they did not present a comparison with experimental values.

In an earlier publication [19], we used the 2CLJQ model of Möller and Fischer [2] to calculate the Joule–Thomson inversion curve (JTIC) of $CO_2$. The JTIC was calculated from different thermodynamic properties (thermal expansivity and compressibility factor) and showed good agreement with experimental values. In this work, we present a comprehensive comparison between calculated values of several thermodynamic properties for $CO_2$ against experimental values as well as against results from the 2CLJQ EOS. We present simulation results for the isobaric heat capacity, volume expansivity, isothermal compressibility, and combinations of these quantities such as the speed of sound and the Joule–Thomson coefficient.

## THERMODYNAMIC PROPERTIES IN THE ISOBARIC–ISOTHERMAL ENSEMBLE

The isobaric–isothermal ensemble partition function, $\Delta$, of a molecular system with $N$ particles at pressure $P$ and temperature $T$ is given in Ref. [20]:

$$\Delta(N,P,T) = \sum_U \sum_V \exp(-\beta U)\exp(-\beta PV)\,\Omega(N,V,U) \tag{1}$$

where $\Omega$ is the microcanonical partition function, $\beta = 1/(k_B T)$, $k_B$ is Boltzmann's constant, $V$ is the system volume and $U$ is the system energy. The average of a property $X$ in this ensemble can be expressed as:

$$\langle X\rangle = \frac{\sum_U \sum_V X\Omega(N,V,U)\exp[-\beta(U+PV)]}{\sum_U \sum_V \exp[-\beta(U+PV)]} \tag{2}$$

Temperature and pressure derivatives of $X$ in the isobaric–isothermal ensemble can be expressed in terms of fluctuations [21,22]:

$$\left(\frac{\partial\langle X\rangle}{\partial\beta}\right)_P = \left\langle\left(\frac{\partial X}{\partial\beta}\right)_P\right\rangle = (\langle X\rangle\langle H\rangle - \langle XH\rangle) \tag{3}$$

$$\left(\frac{\partial\langle X\rangle}{\partial P}\right)_\beta = \left\langle\left(\frac{\partial X}{\partial P}\right)_\beta\right\rangle = \beta(\langle X\rangle\langle V\rangle - \langle XV\rangle) \tag{4}$$

where $H$ is the system enthalpy. From the above equations, it is possible to derive expressions for the volume expansivity, $\beta_P$, the isothermal compressibility, $\kappa$, and the configurational isobaric heat capacity, $C_P^{\mathrm{conf}}$ :

$$\beta_P = \frac{1}{\langle V\rangle}\left(\frac{\partial\langle V\rangle}{\partial T}\right)_P = -\frac{k_B\beta^2}{\langle V\rangle}\left(\frac{\partial\langle V\rangle}{\partial\beta}\right)_P = -\frac{k_B\beta^2}{\langle V\rangle}(\langle V\rangle\langle H\rangle - \langle VH\rangle) \tag{5}$$

$$\kappa = -\frac{1}{\langle V\rangle}\left(\frac{\partial\langle V\rangle}{\partial P}\right)_\beta = -\frac{\beta}{\langle V\rangle}(\langle V\rangle^2 - \langle V^2\rangle) \tag{6}$$

$$C_P^{\mathrm{conf}} = \left(\frac{\partial\langle H\rangle}{\partial T}\right)_P = \left(\frac{\partial\langle U\rangle}{\partial T}\right)_P + P\left(\frac{\partial\langle V\rangle}{\partial T}\right)_P - Nk_B$$
$$= -k_B\beta^2\left(\frac{\partial\langle U\rangle}{\partial\beta}\right)_P - k_B\beta^2 P\left(\frac{\partial\langle V\rangle}{\partial\beta}\right)_P - Nk_B$$
$$C_P^{\mathrm{conf}} = -k_B\beta^2[\langle U\rangle\langle H\rangle - \langle UH\rangle] - k_B\beta^2 P[\langle V\rangle\langle H\rangle - \langle VH\rangle] - Nk_B \tag{7}$$

where $U$ is the configurational energy. The molar configurational isobaric heat capacity can be obtained as $c_P^{\mathrm{conf}} = C_P^{\mathrm{conf}}(N_A/N)$, where $N_A$ is Avogadro's number. To obtain the total isobaric heat capacity it is necessary to add to the above expression the ideal gas heat capacity, $C_P^{\mathrm{ideal}}$ :

$$C_P = C_P^{\mathrm{ideal}} + C_P^{\mathrm{conf}} \tag{8}$$

The ideal gas heat capacity was calculated from the correlation given in Ref. [6] which represents a data set that consider first order corrections to the rigid rotator, harmonic-oscillator model, with deviations less than $\pm 0.02\%$.

From these properties, it is possible to derive other thermodynamic properties of interest, such as the isochoric heat capacity, the Joule–Thomson coefficient and the speed of sound.

The isochoric heat capacity, $C_v$, can be calculated from thermodynamic relations as:

$$C_P - C_v = -T\frac{\left[\left(\frac{\partial\langle V\rangle}{\partial T}\right)_P\right]^2}{\left(\frac{\partial\langle V\rangle}{\partial P}\right)_T} = T\langle V\rangle\frac{\beta_P^2}{\kappa} \quad (9)$$

Finally, the Joule–Thomson coefficient, $\mu_{JT}$, and speed of sound, $u$, can be expressed as:

$$\mu_{JT} = \left(\frac{\partial T}{\partial P}\right)_h = \frac{1}{C_P}\left[T\left(\frac{\partial\langle V\rangle}{\partial T}\right)_P - \langle V\rangle\right] = \frac{\langle V\rangle}{C_P}[T\beta_P - 1] \quad (10)$$

$$u^2 = -\frac{C_P}{C_v}\frac{\langle V\rangle^2}{\left(\frac{\partial\langle V\rangle}{\partial P}\right)_T}\frac{MN_A}{N} = \frac{C_P}{C_v}\frac{MN_A}{N}\frac{\langle V\rangle}{\kappa} \quad (11)$$

where $M$ is the molecular weight. Expressions for other thermodynamic properties, such as the adiabatic expansivity or the Grüneisen parameter can be obtained from combinations of the relations in this section.



## POTENTIAL MODEL

The model of Möller and Fischer for a 2CLJQ fluid [2] was used to describe $CO_2$. A molecule is composed of two identical Lennard–Jones sites a distance $l$ apart plus a point quadrupole moment $Q$ placed in the geometric center of the molecule. The full potential, $u_{2CLJQ}$, is written as:

$$u_{2CLJQ}(\mathbf{r_{ij}}, \boldsymbol{\omega}_\mathbf{i}, \boldsymbol{\omega}_\mathbf{j}, l, Q^2) = u_{2CLJ}(\mathbf{r_{ij}}, \boldsymbol{\omega}_\mathbf{i}, \boldsymbol{\omega}_\mathbf{j}, l) + u_Q(\mathbf{r_{ij}}, \boldsymbol{\omega}_\mathbf{i}, \boldsymbol{\omega}_\mathbf{j}, Q^2) \quad (12)$$

where

$$u_{2CLJ}(\mathbf{r_{ij}}, \boldsymbol{\omega}_\mathbf{i}, \boldsymbol{\omega}_\mathbf{j}, l) = 4\varepsilon\sum_{a=1}^{2}\sum_{b=1}^{2}\left[\left(\frac{\sigma}{r_{ab}}\right)^{12} - \left(\frac{\sigma}{r_{ab}}\right)^{6}\right] \quad (13)$$

and

$$u_Q(\mathbf{r_{ij}}, \boldsymbol{\omega}_\mathbf{i}, \boldsymbol{\omega}_\mathbf{j}, Q^2) = \frac{3}{4}\frac{Q^2}{4\pi\varepsilon_0|\mathbf{r_{ij}}|^5}[1 - 5(c_i^2 + c_j^2) - 15c_i^2c_j^2 + 2(c - 5c_ic_j)^2] \quad (14)$$

In Eq. (13), $r_{ab}$ is one of the four Lennard–Jones site-to-site distances (see Fig. 1a) where $a$ counts the two sites of molecule $i$, and $b$ counts those of molecule $j$. The Lennard–Jones parameters $\sigma$ and $\varepsilon$ represent the size of each site and the well depth of the potential energy, respectively.

The contribution to the potential energy due to the quadrupole–quadrupole interactions is given by Eq. (14), where $\mathbf{r_{ij}}$ is the center-to-center distance between two molecules, $i$ and $j$ (see Fig. 1b). The vectors $\boldsymbol{\omega}_\mathbf{i}$ and $\boldsymbol{\omega}_\mathbf{j}$ represent the orientation of molecules $i$ and $j$; $\theta_i$ and $\theta_j$ are the angles between the axis of the molecule and the center-to-center connection line, and $\phi_{ij}$ is the difference in azimuthal angles of molecules $i$ and $j$. In this equation, $\varepsilon_0$ is the permittivity of free space.

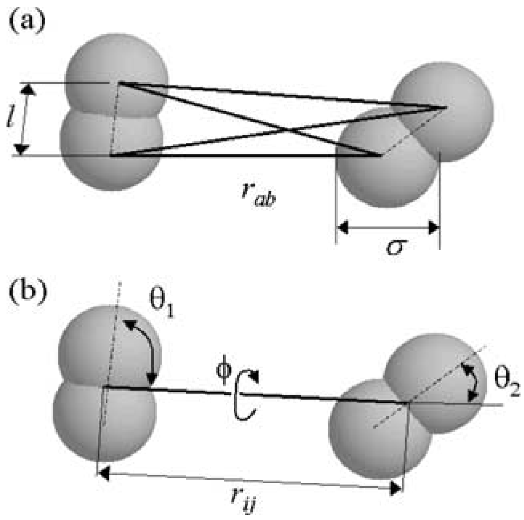


FIGURE 1 Representation of the 2CLJQ model. (a) Each molecule consists of two LJ centers of diameter $\sigma$ separated by a distance $l$. Dispersion–repulsion interactions between the sites are calculated for all distances $r_{ab}$. (b) Point quadrupoles are located at the center of each 2CLJ molecule. Quadrupole–quadrupole interactions between two molecules depend on the orientation of the molecules ($\theta_1$, $\theta_2$, $\phi$) and the distance $r_{ij}$ between the two molecules.

We used potential parameters suggested by Möller and Fischer [2]: $\varepsilon/k_B = 125.317\,\mathrm{K}$, $\sigma = 3.0354\,\text{Å}$, $L = l/\sigma = 0.699$ and $Q^{*2} = Q^2/(4\pi\varepsilon_0\sigma^5) = 3.0255$.

## SIMULATION DETAILS

The fluctuation method based on Monte Carlo simulations in the isothermal–isobaric ensemble was used. Simulations containing 500, 864 and 1320 molecules, initially placed on a face-centered cubic lattice, were performed at low and high temperature, and it was verified that the results were independent on the size of the system. Therefore, the results in this work correspond to a total of $N = 500$ molecules. Periodic boundary conditions and minimum image conventions were applied. Simulations were organized in cycles. Each cycle consisted of $N$ attempts to displace or rotate a randomly chosen molecule and an attempt of volume change. A variable spherical cut-off radius $r_c$, equal to half the box length was used (e.g. at 330.39 K and $P = 2.5\,\mathrm{MPa}$, $r_c = 15.5\sigma = 4.7\,\mathrm{nm}$, and at 330.39 K and $P = 72.3\,\mathrm{MPa}$, $r_c = 5.4\sigma = 1.6\,\mathrm{nm}$), and long-range corrections were recalculated after each volume

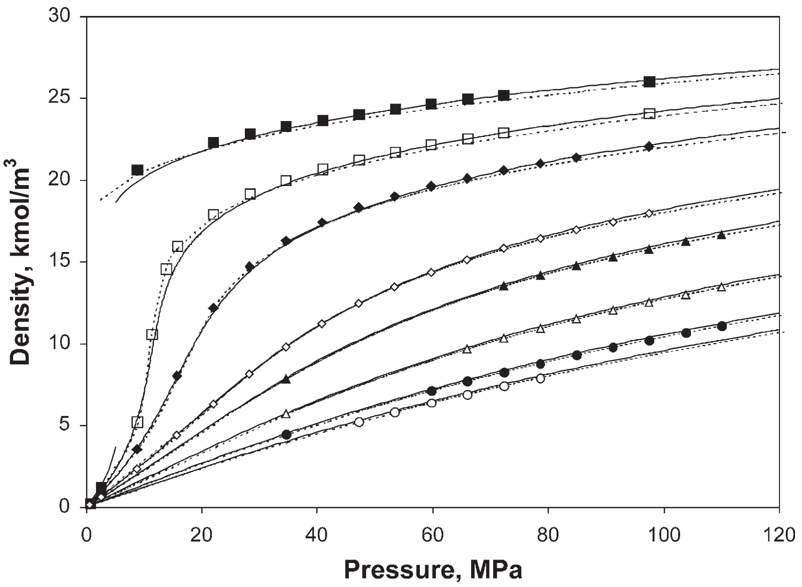


FIGURE 2 Density vs. pressure diagram for carbon dioxide. Continuous lines predicted by the Span–Wagner EOS [6], dashed lines predicted by the 2CLJQ EOS [3–5], and symbols this work: (■) 288.37 K, (□) 330.39 K, (◆) 374.31 K, (◇) 478.71 K, (▲) 546.83 K, (△) 692.60 K, (●) 855.57 K and (○) 952.33 K.



change assuming an homogeneous density for $r > r_c$. Acceptance probabilities of displacement and volume changes were adjusted to be about 30%. Averages were taken over $5 \times 10^5$ cycles, after a stabilization period of at least $3 \times 10^5$ cycles.

## RESULTS

### Results for Volumetric Properties

Figure 2 shows the simulated densities as a function of pressure in comparison with the values predicted from the Span–Wagner EOS and the 2CLJQ EOS for eight isotherms, one of them ($T = 288.37$ K) corresponding to the sub-critical region. This figure shows an excellent agreement between the 2CLJQ EOS and our simulations results, except at the highest densities. Stoll *et al.* [23] carried out an extensive comparison of molecular simulation results of 30 individual 2CLJQ fluids, with different values of $L$ and $Q^{*2}$, against the 2CLJQ EOS. It should be mentioned that the quadrupolar contribution of the 2CLJQ EOS is assumed to be $L$ independent and was obtained for $L = 0.505$. They observed increasing deviations in the VLE predictions for fluids as $L$ departs from 0.505; in particular, they found that the EOS systematically under-predicts the saturated liquid densities and the critical flatness of the phase envelope. Figure 2 shows that the 2CLJQ EOS for

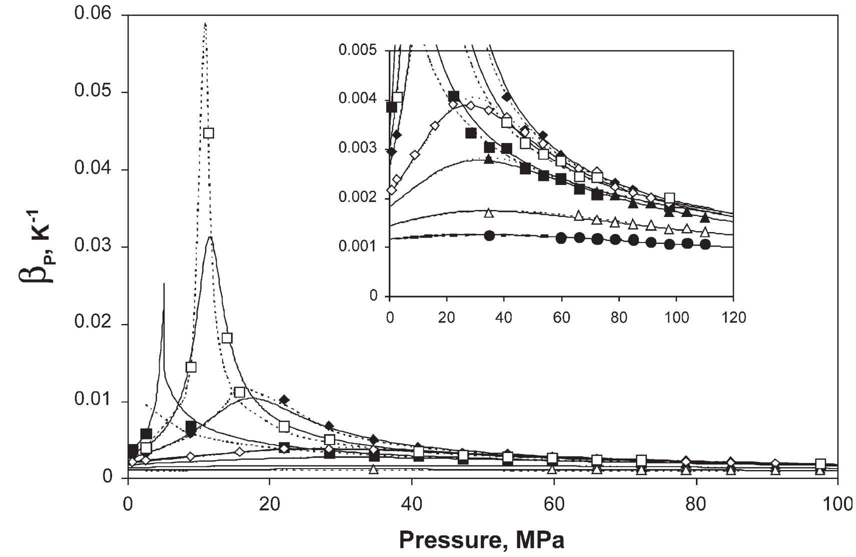


FIGURE 3 Volume expansivity ($\beta_P$) vs. pressure. Legend as in Fig. 2.

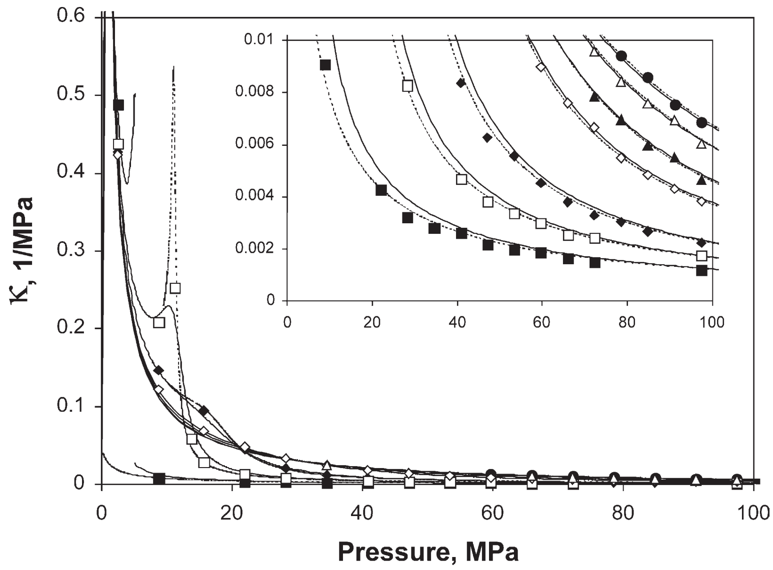


FIGURE 4 Isothermal compressibility ($\kappa$) as a function of pressure. Legend as in Fig. 2.



$CO_2$ ($L = 0.699$) does predict lower densities, especially on the liquid-like branch of the subcritical isotherm studied ($T = 288.37$ K), but the agreement between simulation results and the 2CLJQ EOS improves in the supercritical region, especially at the higher temperatures and pressures.

In general, good agreement is also found between these results and the predictions of the Span and Wagner EOS, except in the extended critical region where deviations in densities up to 5% can be found. The extended critical region includes a temperature range of 20 K and a pressure range of 10 MPa around the critical point. Möller and Fischer obtained similar results from constant pressure–constant temperature molecular dynamics simulations in this region.

The volume expansivity ($\beta_P$) and the isothermal compressibility ($\kappa$) as functions of pressure are shown in Figs. 3 and 4, respectively. The discrepancies between the 2CLJQ model (both simulations and EOS) and the Span–Wagner EOS are obvious in the extended critical region for both quantities. The volume expansivity is overpredicted by the 2CLJQ model by more than 90% at 330 K, as shown by comparison with the Span–Wagner EOS, and even at 288 and 374 K deviations up to 80% can be found. However, these deviations are not surprising since it is known that these derivatives, as well as other properties such as heat capacities, diverge at the critical point, so that any discrepancies between the molecular model and the Span–Wagner EOS are bound to be greatly magnified in this region. In fact, it is known that the 2CLJQ model fails to reproduce the critical point of $CO_2$ exactly; from the correlations developed by Stoll *et al.* [23] for the 2CLJQ fluid, we expect for $CO_2$ a model-predicted critical temperature $T_c = 307.83$ K from simulations and $T_c = 318.4$ K from the 2CLJQ EOS, higher than the accepted experimental value $T_c = 304.128$ K which the Span–Wagner EOS is designed to reproduce. Thus, for instance, for $CO_2$ at 330.39 K the 2CLJQ model gives results that are more near-critical (reduced temperature $T_r = T^*/T_c^* = 1.07$) than in the actual case ($T_r = 1.09$). The corresponding "spikes" in the isotherms in Figs. 3 and 4 are therefore more pronounced for the 2CLJQ model than for the Span–Wagner EOS. A substantially closer agreement between both sets of data would be obtained by computing the isotherms from the reference EOS at the same *reduced* temperature as the simulations.

On the other hand, these differences become less significant at higher temperatures and pressures, away from the extended critical region. At pressures above 40 MPa the agreement between the Span–Wagner EOS and the 2CLJQ model is very good for all temperatures; for temperatures higher than 374 K the agreement is excellent in the entire range of pressures as can be seen in the inset of Fig. 3. A similar behavior for the isothermal compressibility is shown in Fig. 4 (and the inset therein).

Figure 5 illustrates the isobaric heat capacity obtained in this work as a function of density. We have chosen to plot these results (as well as those in the following figures) in terms of density for visual clarity, but the analysis from a $C_P$ vs. $P$ plot shows the same tendency. Deviations smaller than 3% are found between the 2CLJQ model and the Span–Wagner EOS except in the already mentioned extended critical region. Nevertheless, the deviations of $C_P$ in the extended critical region are considerably

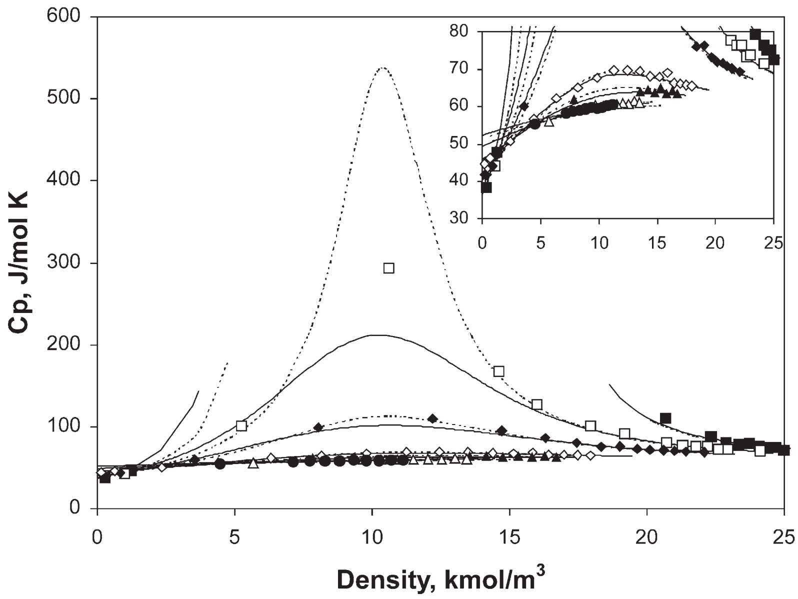


FIGURE 5 Isobaric heat capacity ($C_P$) as a function of density. Legend as in Fig. 2.



smaller than those found for the isothermal compressibility ($\kappa$) and the volume expansivity ($\beta_P$). It is interesting to notice that $\kappa$ and $\beta_P$ involve fluctuations in volume whereas $C_P$ only involves fluctuation in energy and enthalpy.

## Results for Derived Properties

Joule–Thomson coefficients are plotted in Fig. 6 as a function of density. In this case, excellent agreement is found in the entire region of study except at very low densities. Lagache *et al.* [21] recently reported similar results for the low-density region in simulations of methane, ethane and butane with a united atom potential.

The inset in Fig. 6 shows the points obtained in the region where this coefficient changes in sign. The locus of states where the Joule–Thomson coefficient is equal to zero is called the JTIC. The determination of this curve is considered one of the most demanding tests that can be performed on any EOS. In a previous work [19], we obtained the JTIC for $CO_2$, using the same 2CLJQ potential as in the present work. Very good agreement was obtained with both experimental data and molecular simulations, and the work helped to resolve an apparent anomaly in the JTIC that had been reported in the literature.

Finally, in Fig. 7 the speed of sound is plotted against density. The representation of speed of sound

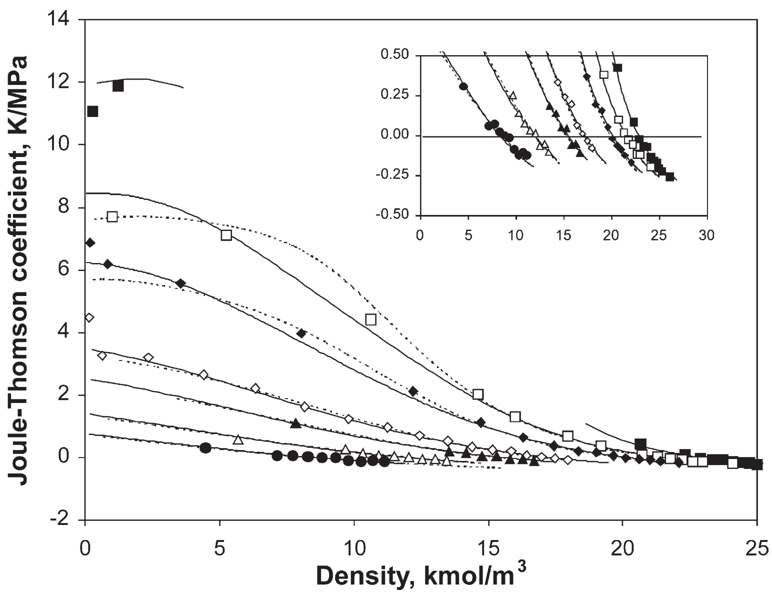


FIGURE 6 Joule–Thomson coefficient vs. density diagram for carbon dioxide. Legend as in Fig. 2.

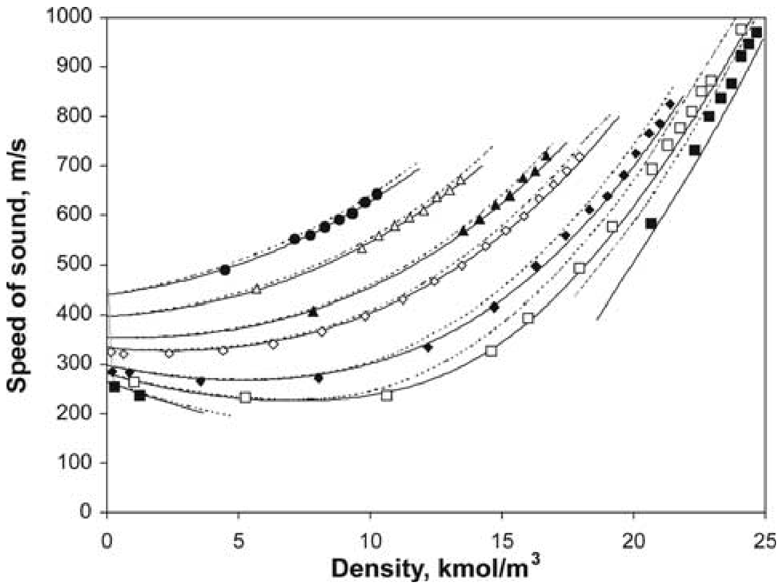


FIGURE 7 Speed of sound vs. density diagram for carbon dioxide. Legend as in Fig. 2.



is regarded as a sensitive test since it involves not only the correct representation of heat capacities, but also of the first derivatives of the volume. The overall predictions can be considered excellent. The largest deviations are once more found for the lower temperature high-density region. These deviations are consistent with the deviations found in density. The largest error in the speed of sound is approximately 5%, which is considerably lower than the errors found in the properties involved in its definition, $C_P$ and $\kappa$ [see Eq. (11)], in the extended critical region, possibly due to a compensation of errors in the quotient of these two quantities. This suggests that speed of sound as a single property may provide a less sensitive test than heat capacity and isothermal compressibility, each by itself, particularly in the near-critical region. For instance, $CO_2$ at 330 K is sufficiently close to critical conditions that a clearly defined peak is observed in $\kappa$ (Fig. 4) and $C_P$ (Fig. 5), yet there is no equivalent minimum in $u$ (Fig. 7), which requires a lower temperature to appear.

## CONCLUSIONS

The parameters for the 2CLJQ model for $CO_2$ were obtained by Möller and Fischer [2] by fitting experimental saturation properties. It has been shown that these parameters give good predictions of VLE properties [2]. In this work, the transferability of the parameters to the supercritical region has been studied through a comprehensive comparison between calculated values of several thermodynamic properties for $CO_2$ and their experimental values (represented by the Span–Wagner EOS) as well as against the 2CLJQ EOS. We have presented simulation results for the isobaric heat capacity, volume expansivity, isothermal compressibility and combinations of these quantities such as the speed of sound and the Joule–Thomson coefficient for which experimental data are available.

It has been shown that these parameters can be used with confidence for the prediction of thermodynamic properties, including those of industrial interest such as the speed of sound or Joule–Thomson coefficient, for $CO_2$ in the supercritical region, except in the extended critical region. This region is larger than usual due to the differences between the critical point predicted for the 2CLJQ model for $CO_2$ and the experimental critical point. Unfortunately, this region is extremely important for the so-called $CO_2$-driven process where the tunability of $CO_2$ plays a key role. Therefore, care must be taken when using this potential to model $CO_2$ in this extended critical region.

We also show that the agreement of calculated and experimental values for speed of sound does not necessarily guarantees good agreement in the isobaric heat capacity and the first derivatives of the volume.

Deviations between the 2CLJQ EOS and simulations, which can be quite large in the two-phase region [22], appear to become less important at higher supercritical temperatures and pressures. The present results, however, are limited to $CO_2$ only. More extensive testing with a wider range of fluids will be required before the predictive capabilities of the 2CLJQ can be fully assessed in the supercritical region.

## *Acknowledgements*

This work was supported in part by the STC Program of the National Science Foundation under Agreement No. CHE 9876674, and by the Grant Agency of the Czech Republic under Grant No. 203/02/0805.


## *References*


[1] Kronome, G., Kristóf, T., Liszi, J. and Szalai, I. (1999) "Heat capacities of two-centre Lennard–Jones fluid from NpT ensemble Monte Carlo simulations", *Fluid Phase Equilib.* **155**, 157.

[2] Möller, D. and Fischer, J. (1994) "Determination of an effective intermolecular potential for carbon-dioxide using vapor liquid-phase equilibria from NPT plus test particle simulations", *Fluid Phase Equilib.* **100**, 35.

[3] Mecke, M., Müller, A., Winkelmann, J. and Fischer, J. (1997) "An equation of state for two-center Lennard–Jones fluids", *Int. J. Thermophys.* **18**(3), 683.

[4] Mecke, M., Müller, A., Winkelmann, J. and Fischer, J. (1998) "Erratum 2", *Int. J. Thermophys.* **19**(5), 1495.

[5] Saager, B. and Fischer, J. (1992) "Construction and application of physically based equations of state Part II. The dipolar and quadrupolar contributions to the Helmholtz energy", *Fluid Phase Equilib.* **72**, 67.

[6] Span, R. and Wagner, W. (1996) "A new equation of state for carbon dioxide covering the fluid region from the triple-point temperature to 1100 K at pressures up to 800 MPa", *J. Phys. Chem. Ref. Data* **25**, 1509.

[7] Harris, J.G. and Yung, K.H. (1995) "Carbon dioxide's liquid–vapor coexistence curve and critical properties as predicted by a simple molecular model", *J. Phys. Chem.* **99**, 12021.

[8] Potoff, J.J., Errington, J.R. and Panagiotopoulos, A.Z. (1999) "Molecular simulations of phase equilibria for mixtures of polar and non-polar components", *Mol. Phys.* **97**, 1073.

[9] Vrabec, J., Stoll, J. and Hasse, H. (2001) "A set of molecular models for symmetric quadrupolar fluids", *J. Phys. Chem. B* **105**, 12126.

[10] Singer, K., Taylor, A. and Singer, J.V.L. (1977) "Thermodynamic and structural properties of liquids modeled by 2-Lennard–Jones centers pair potentials", *Mol. Phys.* **33**, 1757.

[11] Murthy, C.S., O'Shea, S.F. and McDonald, I.R. (1983) "Electrostatic interactions in molecular crystals. Lattice dynamics of solid nitrogen and carbon dioxide", *Mol. Phys.* **50**, 531.

[12] Yang, J., Ren, Y., Tian, A. and Sun, H. (2000) "COMPASS force field for 14 inorganic molecules, He, Ne, Ar, Kr, Xe, $H_2$, $O_2$, $N_2$, NO, CO, $CO_2$, $NO_2$, $CS_2$, and $SO_2$, in liquid phases", *J. Phys. Chem. B* **104**, 4951.

[13] Potoff, J.J. and Siepmann, J.I. (2000) "Vapor–liquid equilibria of mixtures containing alkanes, carbon dioxide, and nitrogen", *AICHE J.* **47**(7), 1676.

[14] Fotouh, K. and Shukla, K. (1997) "Effect of quadrupole moment on excess properties of binary 2CLJQ mixtures from molecular dynamics simulation: model and real mixtures", *Fluid Phase Equilib.* **135**, 35.

[15] Vrabec, J. and Fischer, J. (1997) "Vapor–liquid equilibria of the ternary mixture $CH_4 + C_2H_6 + CO_2$ from molecular simulation", *AIChE J.* **43**, 212.

[16] Vrabec, J. and Fischer, J. (1996) "Vapor–liquid equilibria of binary mixtures containing methane, ethane, and carbon dioxide from molecular simulation", *Int. J. Thermophys.* **17**, 889.

[17] De Santis, A., Frattini, R., Gazzillo, D. and Sampoli, M. (1987) "The potential model dependence of the neutron radial and partial distribution functions for liquid $CO_2$", *Mol. Phys.* **60**, 21.

[18] Chen, B., Siepmann, J.I. and Klein, M.L. (2001) "Direct Gibbs ensemble Monte Carlo simulations for solid–vapor phase equilibria: applications to Lennard–Jonesium and carbon dioxide", *J. Phys. Chem. B* **105**, 9840.

[19] Colina, C.M., Lísal, M., Siperstein, F.R. and Gubbins, K.E. (2002) "Accurate $CO_2$ Joule–Thomson inversion curve by molecular simulations", *Fluid Phase Equilib.* **202**, 253.

[20] McQuarrie, D.A. (1976) *Statistical Mechanics* (HarperCollins, New York).

[21] Lagache, M., Ungerer, P., Boutin, A. and Fuchs, A.H. (2001) "Prediction of thermodynamic derivative properties of fluids by Monte Carlo simulation", *PCCP* **3**, 4333.

[22] Kronome, G., Liszi, J. and Szalai, I. (1998) "Monte Carlo simulation of some thermophysical properties of two-centre Lennard–Jones fluids along the vapour–liquid equilibrium curve", *Mol. Phys.* **93**, 279.

[23] Stoll, J., Vrabec, J., Hasse, H. and Fischer, J. (2001) "Comprehensive study of the vapour–liquid equilibria of the pure two-centre Lennard–Jones plus pointquadrupole fluid", *Fluid Phase Equilib.* **179**, 339.